Capacitor voltage ripple and capacitance evaluation in a direct three-phase to single-phase ac/ac MMC

Capacitor voltage ripple and capacitance evaluation in a direct three-phase to single-phase ac/ac MMC

Ygor Pereira Marca, Maurice G. L. Roes and Korneel G. E. Wijnands
Department of Electrical Engineering, Electromechanics and Power Electronics Group
Eindhoven University of Technology, Eindhoven, The Netherlands
Email: y.pereira.marca@tue.nl

***Abstract*—This paper introduces the capacitor current and voltage ripple evaluation of a direct three-phase to single-phase ac/ac modular multilevel converter with full-bridge sub-modules. Based a desired sub-module capacitor voltage ripple, the required capacitance is calculated, which is valuable to dimension sub-modules' energy storage in many applications. Simulations and measurements using a scaled-down prototype validate the analysis.**

***Index Terms*—battery, capacitance, capacitor RMS current, capacitor voltage ripple, full-bridge, medium-voltage, MMC.**

I. Introduction

Ultrafast chargers based on direct ac/ac modular multilevel converters (MMCs) reduce the size and cost of medium-voltage (MV) connected chargers by employing a single medium-frequency transformer (MFT) [1]–[3]. However, the MMC sub-module (SM) capacitors are still a driving factor of the converter's volume and price [4]–[6]. In addition, MMC SMs must keep an admissible current ripple, and therefore voltage ripple, to minimize capacitor loss [7]. Increasing SMs capacitance reduces the voltage ripple. Based on a desired capacitor voltage ripple, the desired sub-module capacitance can be estimated [8]–[14].

The ac/dc modular multilevel converter has a capacitor voltage ripple that is dominated by the grid second-order harmonic frequency [15]–[17]. The voltage ripple related to the grid frequency can be decreased through a control scheme [18]–[21]. Despite that, the medium-frequency single-phase voltage output of the ac/ac MMC adds higher-order harmonics to the capacitor current and voltage ripple [1], [2]. Therefore, this paper investigates SM capacitor current, voltage ripple and the necessary capacitance to maintain the ripple within desired limits in an ac/ac MMC with full-bridge SMs.

II. Modular multilevel converter

The MMC with full-bridge SMs offers ac/dc and ac/ac conversion between the three-phase and single-phase terminals [1], [2], [6], [17]. The ac/ac MMC is for example able to connect a MV grid to a MFT, with frequencies $\omega_1 = 2\pi f_1$ and $\omega_2 = 2\pi f_2$, respectively. As shown in Fig. 1, a transformer connected to the single-phase terminals can offer galvanic isolation between the three-phase ac voltage (u_y) and the dc voltage (u_{dc}). In the MMC the upper and lower arms are denoted by $\mathrm{x} \in \{\mathrm{u}, \mathrm{l}\}$ and three phase quantities are indicated by $y \in \{a,\ b,\ c\}$. The arms are comprised of a series inductance L_y and N series-connected SMs, each comprised of a full-bridge converter and a dc-bus capacitor.

A. Fundamentals

The series connected SMs in a MMC arm can be simplified to controllable voltage and current sources (Fig. 2), representing the average behavior [1], [2]. Therefore, SMs from each arm are combined to create the summed capacitor voltages $\mathrm{v}_y^{\mathrm{x}} = \sum_{k=1}^{N} \mathrm{v}_{y,k}^{\mathrm{x}}$ as in Fig. 2, where $\mathrm{v}_{y,k}^{\mathrm{x}}$ is the SM capacitor voltage of the k^{th} sub-module. Additionally, the SMs capacitor voltages are related to the arm voltages $u_y^{\mathrm{x}} = \sum_{k=1}^{N} S_{y,k}^{\mathrm{x}}\, \mathrm{v}_{y,k}^{\mathrm{x}}$, with the k^{th} SM's switching function given by $S_{y,k}^{\mathrm{x}} \in \{-1, 0, 1\}$. The switching functions generate the arms' average insertion indices $n_y^{\mathrm{x}} = \frac{1}{N} \sum_{k=1}^{N} S_{y,k}^{\mathrm{x}}$, where $-1 \leq n_y^{\mathrm{x}} \leq 1$, leading to $u_y^{\mathrm{x}} = n_y^{\mathrm{x}} \mathrm{v}_y^{\mathrm{x}}$.

Assuming that the SM capacitors in each arm have equal capacitance, the equivalent capacitance in the arms $C_\sigma = \frac{C_y}{N}$ decreases as the number of SMs increases. Assuming that the capacitor voltages are equal for every module in the arm, the insertion indices steer the voltage and current sources in Fig. 2 as $u_y^{\mathrm{x}} = n_y^{\mathrm{x}} \mathrm{v}_y^{\mathrm{x}}$ and $\imath_{Cy}^{\mathrm{x}} = n_y^{\mathrm{x}} \imath_y^{\mathrm{x}}$.

B. Decomposition of the circuit states

The MMC arm voltages and currents can be decomposed into differential-mode (Δ) and common-mode components (Σ) as

$$u_y^{\Delta} = \frac{1}{2}\left(u_y^{\mathrm{u}} - u_y^{\mathrm{l}}\right), \tag{1}$$

$$\imath_y^{\Delta} = \frac{1}{2}\left(\imath_y^{\mathrm{u}} - \imath_y^{\mathrm{l}}\right), \tag{2}$$

$$u_y^{\Sigma} = \frac{1}{2}\left(u_y^{\mathrm{u}} + u_y^{\mathrm{l}}\right), \tag{3}$$

$$\imath_y^{\Sigma} = \frac{1}{2}\left(\imath_y^{\mathrm{u}} + \imath_y^{\mathrm{l}}\right). \tag{4}$$

Assuming sinusoidal PWM modulation, the steady-state differential-mode components are defined as

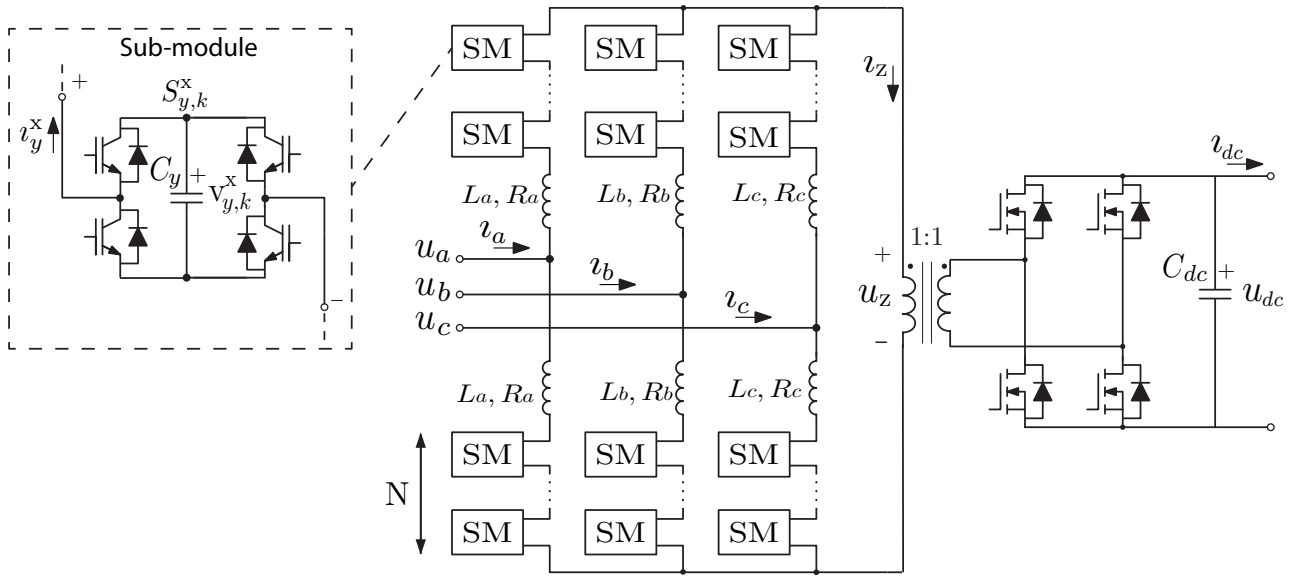

Fig. 1. Electrical circuit of a MMC-based ultrafast charger.

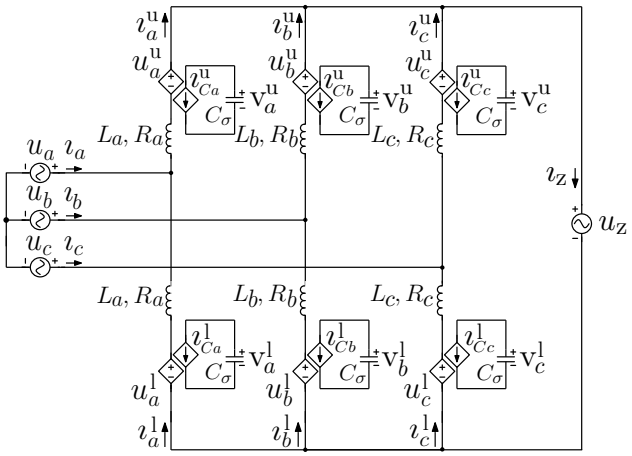

Fig. 2. Three-phase to single-phase ac/ac MMC averaged equivalent circuit.

$$u_y^{\Delta} = -\sqrt{2}U_y^{\Delta}\cos\left(\omega_1 t + \theta_y^{\Delta}\right), \tag{5}$$

$$\imath_y^{\Delta} = \sqrt{2}I_y^{\Delta}\cos\left(\omega_1 t + \varphi_y^{\Delta}\right), \tag{6}$$

where ω_1 is the grid frequency.

The steady-state common-mode components are described as

$$u_y^{\Sigma} = \sqrt{2}U_{y1}^{\Sigma}\cos\left(\omega_1 t + \theta_{y1}^{\Sigma}\right) + \sqrt{2}U_{y2}^{\Sigma}\cos\left(\omega_2 t + \theta_{y2}^{\Sigma}\right), \tag{7}$$

$$\imath_y^{\Sigma} = \sqrt{2}I_{y1}^{\Sigma}\cos\left(\omega_1 t + \varphi_{y1}^{\Sigma}\right) + \sqrt{2}I_{y2}^{\Sigma}\cos\left(\omega_2 t + \varphi_{y2}^{\Sigma}\right), \tag{8}$$

where ω_2 is the fundamental frequency of the single-phase voltage and current u_{z} and $\imath_{\mathrm{z}}$. These definitions offer a decoupled control between grid and MFT currents [2].

C. Power distribution

Based on this decomposition, the instantaneous power $p_y^{\mathrm{x}} = -u_y^{\mathrm{x}}\imath_y^{\mathrm{x}}$ processed by the controllable voltage source of each MMC arm in Fig. 2 is defined as $p_y^{\Sigma} = \frac{1}{2}\left(p_y^{\mathrm{u}} + p_y^{\mathrm{l}}\right)$ and $p_y^{\Delta} = \frac{1}{2}\left(p_y^{\mathrm{u}} - p_y^{\mathrm{l}}\right)$. The time averaged common and differential-mode powers are given by $P_y^{\Sigma} = U_y^{\Delta}I_y^{\Delta}\cos\left(\theta_y^{\Delta} - \varphi_y^{\Delta}\right) - U_{y2}^{\Sigma}I_{y2}^{\Sigma}\cos\left(\theta_{y2}^{\Sigma} - \varphi_{y2}^{\Sigma}\right)$ and $P_y^{\Delta} = -U_{y1}^{\Sigma}I_y^{\Delta}\cos\left(\theta_y^{\Delta} - \varphi_y^{\Delta}\right)$, respectively. The average power P_y^{Σ} is equal to zero in steady-state due to equal power flowing in and out of the three-phase and single-phase ports. In addition, P_y^{Δ} is regulated by U_{y1}^{Σ}, with in steady-state $U_{y1}^{\Sigma} = 0$ and therefore $I_{y1}^{\Sigma} = 0$. Furthermore, P_y^{Σ} and P_y^{Δ} can be controlled through u_{y1}^{Σ} and u_{y2}^{Σ} respectively [2]. The control scheme to regulate common-mode voltages is not investigated in this paper, but it can be found in [1], [17].

D. Arm capacitor current and voltage ripple

The SM capacitor current and voltage ripple calculation are necessary for capacitor dimensioning in any MMC application. Without loss of generality, the capacitor current and voltage ripple of the upper arms is calculated from Fig. 2. The ripples for the lower arms are equal due to symmetry. The upper arm insertion indices and the average summed capacitor voltage are found to be

$$n_y^{\mathrm{u}} = \frac{u_y^{\Delta} + u_y^{\Sigma}}{\mathrm{V}_y^{\mathrm{u}}}, \tag{9}$$

$$\mathrm{V}_y^{\mathrm{u}} = \widehat{U}_y + \frac{\widehat{U}_{\mathrm{z}}}{2}, \tag{10}$$

where $\widehat{U}_y$ and $\widehat{U}_{\mathrm{z}}$ are the voltage amplitudes of the grid and MFT. The capacitor voltage ripple can be reduced by appropriate choice of the modulation scheme to obtain (9) [22]. However, this paper does not cover modulation, as it focuses on analytical expressions for the capacitor current

and voltage ripple based on the MMC averaged equivalent circuit. During steady-state $U_{y1}^{\Sigma}=0$, therefore

$$n_y^{\mathrm{u}} = -\sqrt{2}\frac{U_y^{\Delta}}{\mathrm{V}_y^{\mathrm{u}}}\cos(\omega_1 t+\theta_y^{\Delta}) + \sqrt{2}\frac{U_{y2}^{\Sigma}}{\mathrm{V}_y^{\mathrm{u}}}\cos(\omega_2 t+\theta_{y2}^{\Sigma}). \tag{11}$$

In addition, based on the common and differential-mode decomposition, the SM capacitor currents are

$$\begin{aligned} i_{Cy}^{\mathrm{u}} =& -\frac{U_y^{\Delta}}{\mathrm{V}_y^{\mathrm{u}}}I_y^{\Delta}\cos(2\omega_1 t+\theta_y^{\Delta}+\varphi_y^{\Delta}) \\ &+\frac{U_{y2}^{\Sigma}}{\mathrm{V}_y^{\mathrm{u}}}I_{y2}^{\Sigma}\cos(2\omega_2 t+\theta_{y2}^{\Sigma}+\varphi_{y2}^{\Sigma}) \\ &-\frac{U_y^{\Delta}}{\mathrm{V}_y^{\mathrm{u}}}I_{y2}^{\Sigma}\cos[(\omega_1+\omega_2)t+\theta_y^{\Delta}+\varphi_{y2}^{\Sigma}] \\ &+\frac{U_{y2}^{\Sigma}}{\mathrm{V}_y^{\mathrm{u}}}I_y^{\Delta}\cos[(\omega_1+\omega_2)t+\theta_{y2}^{\Sigma}+\varphi_y^{\Delta}] \\ &-\frac{U_y^{\Delta}}{\mathrm{V}_y^{\mathrm{u}}}I_{y2}^{\Sigma}\cos[(\omega_1-\omega_2)t+\theta_y^{\Delta}-\varphi_{y2}^{\Sigma}] \\ &+\frac{U_{y2}^{\Sigma}}{\mathrm{V}_y^{\mathrm{u}}}I_y^{\Delta}\cos[(\omega_2-\omega_1)t+\theta_{y2}^{\Sigma}-\varphi_y^{\Delta}], \end{aligned} \tag{12}$$

considering the dc currents equal to zero in steady-state. To evaluate the steady-state summed capacitor voltage ripple, the integral of (12) results in

$$\begin{aligned} \mathrm{v}_y^{\mathrm{u}} =& \mathrm{V}_y^{\mathrm{u}} - \frac{1}{2\omega_1 C_\sigma}\frac{U_y^{\Delta}}{\mathrm{V}_y^{\mathrm{u}}}I_y^{\Delta}\sin(2\omega_1 t+\theta_y^{\Delta}+\varphi_y^{\Delta}) \\ &+\frac{1}{2\omega_2 C_\sigma}\frac{U_{y2}^{\Sigma}}{\mathrm{V}_y^{\mathrm{u}}}I_{y2}^{\Sigma}\sin(2\omega_2 t+\theta_{y2}^{\Sigma}+\varphi_{y2}^{\Sigma}) \\ &-\frac{1}{(\omega_1+\omega_2)C_\sigma}\frac{U_y^{\Delta}}{\mathrm{V}_y^{\mathrm{u}}}I_{y2}^{\Sigma}\sin\left[(\omega_1+\omega_2)t+\theta_y^{\Delta}+\varphi_{y2}^{\Sigma}\right] \\ &+\frac{1}{(\omega_1+\omega_2)C_\sigma}\frac{U_{y2}^{\Sigma}}{\mathrm{V}_y^{\mathrm{u}}}I_y^{\Delta}\sin\left[(\omega_1+\omega_2)t+\theta_{y2}^{\Sigma}+\varphi_y^{\Delta}\right] \\ &-\frac{1}{(\omega_1-\omega_2)C_\sigma}\frac{U_y^{\Delta}}{\mathrm{V}_y^{\mathrm{u}}}I_{y2}^{\Sigma}\sin\left[(\omega_1-\omega_2)t+\theta_y^{\Delta}-\varphi_{y2}^{\Sigma}\right] \\ &+\frac{1}{(\omega_2-\omega_1)C_\sigma}\frac{U_{y2}^{\Sigma}}{\mathrm{V}_y^{\mathrm{u}}}I_y^{\Delta}\sin\left[(\omega_2-\omega_1)t+\theta_{y2}^{\Sigma}-\varphi_y^{\Delta}\right]. \end{aligned} \tag{13}$$

The summed capacitor voltage ripple contains the same frequency components as its current. The voltage ripple depends on the averaged summed capacitor voltage, arm capacitance, common- and differential-mode voltage and current, frequencies $2\omega_1$, $2\omega_2$, $\omega_1+\omega_2$ and $\omega_2-\omega_1$ and all the angles in (13). Thus, the frequency with the greatest amplitude in the capacitor voltage ripple depends on the application. For instance, ultrafast chargers consider $\omega_2 > \omega_1$ to diminish the MFT size and cost [1]–[3]. In that case, the double frequency ($2\omega_1$) from the grid has more influence on the capacitor voltage ripple than the double frequency ($2\omega_2$) from the MFT. However, in traction systems the double frequency ($2\omega_2$) from the MFT has more influence on the capacitor voltage ripple since in this application $\omega_1 > \omega_2$ [17].

III. Capacitance Evaluation

The SM capacitor RMS current and voltage ripple are necessary to dimension the MMC energy storage requirements. The RMS current is obtained from the amplitudes of the components in (12). The amplitudes with frequencies $2\omega_1$ ($\hat{I}_{Cy,2\omega_1}^{\mathrm{u}}$) and $2\omega_2$ ($\hat{I}_{Cy,2\omega_2}^{\mathrm{u}}$) are straightforward. The amplitudes with frequencies $\omega_1+\omega_2$ ($\hat{I}_{Cy,\omega_1+\omega_2}^{\mathrm{u}}$) and $\omega_2-\omega_1$ ($\hat{I}_{Cy,\omega_2-\omega_1}^{\mathrm{u}}$) need manipulation. The SM capacitor RMS current is given by

$$I_{Cy}^{\mathrm{u}} = \left\{ \frac{\left(\hat{I}_{Cy,2\omega_1}^{\mathrm{u}}\right)^2+\left(\hat{I}_{Cy,2\omega_2}^{\mathrm{u}}\right)^2}{2} + \frac{\left(\hat{I}_{Cy,\omega_1+\omega_2}^{\mathrm{u}}\right)^2+\left(\hat{I}_{Cy,\omega_2-\omega_1}^{\mathrm{u}}\right)^2}{2} \right\}^{\frac{1}{2}}. \tag{14}$$

In addition, (13) can be used to specify the SM capacitance for a desired voltage ripple ($\Delta\mathrm{V}_y^{\mathrm{x}}$) in ac/ac MMCs with full-bridge SMs. A theoretical upper limit to the voltage ripple can be derived by considering all components to have a phase such that their peaks align.

$$\begin{aligned} C_y^{lim} =& \frac{2N}{\nu\left(\mathrm{V}_y^{\mathrm{x}}\right)^2}\left[\frac{U_y^{\Delta}I_y^{\Delta}}{2\omega_1}+\frac{U_{y2}^{\Sigma}I_{y2}^{\Sigma}}{2\omega_2}\right] \\ &+\frac{2N}{\nu\left(\mathrm{V}_y^{\mathrm{x}}\right)^2}\left[\frac{U_{y2}^{\Sigma}I_y^{\Delta}+U_y^{\Delta}I_{y2}^{\Sigma}}{\omega_1+\omega_2}\right] \\ &+\frac{2N}{\nu\left(\mathrm{V}_y^{\mathrm{x}}\right)^2}\left[\frac{U_{y2}^{\Sigma}I_y^{\Delta}+U_y^{\Delta}I_{y2}^{\Sigma}}{\omega_2-\omega_1}\right]. \end{aligned} \tag{15}$$

This is the worst case voltage ripple that can occur. Here $\nu=\frac{\Delta\mathrm{V}_y^{\mathrm{x}}}{\mathrm{V}_y^{\mathrm{x}}}$ is the ratio of peak-to-peak voltage ripple to average summed capacitor voltage. If $\omega_2 \gg \omega_1$, the capacitor ripple in (13) can be approximated by only the first sine term, leading to a required capacitance

$$C_y = \frac{U_y^{\Delta}I_y^{\Delta}N}{\omega_1\nu\left(\mathrm{V}_y^{\mathrm{x}}\right)^2}. \tag{16}$$

IV. Experimental Verification

Simulations and experiments were conducted with the parameters described in Table I. Simulations were performed with the switched and averaged models from Fig. 1 and Fig. 2, respectively. Experiments were carried out with a scaled-down prototype shown in Fig. 3.

To calculate current amplitudes in (14), $I_y^{\Delta}=\frac{P_{out}}{6U_y}$, $U_y^{\Delta}=\sqrt{(U_y)^2+\left(\omega_1 L_y I_y^{\Delta}\right)^2}$, $\theta_y^{\Delta}=\arcsin\left(\frac{\omega_1 L_y I_y^{\Delta}}{U_y^{\Delta}}\right)$ and $\varphi_y^{\Delta}=0$ are fixed for an unitary power factor. To evaluate (14), $I_{y2}^{\Sigma}=\frac{P_{out}}{6U_{y2}^{\Sigma}}$, $U_{y2}^{\Sigma}=\frac{U_z}{2}$, $\theta_{y2}^{\Sigma}=0$ and φ_{y2}^{Σ} can be imposed by means of a closed-loop control [1], [17]. The current amplitudes and the RMS current in (14) are plotted in relation to φ_{y2}^{Σ} as shown in Fig. 4. To reduce SM capacitor RMS current, the control must impose an angle φ_{y2}^{Σ} that results in the I_{Ca}^{u} curve valley in Fig 4.

The RMS capacitor current in (14) is plotted in relation to the MMC output power together with measurements

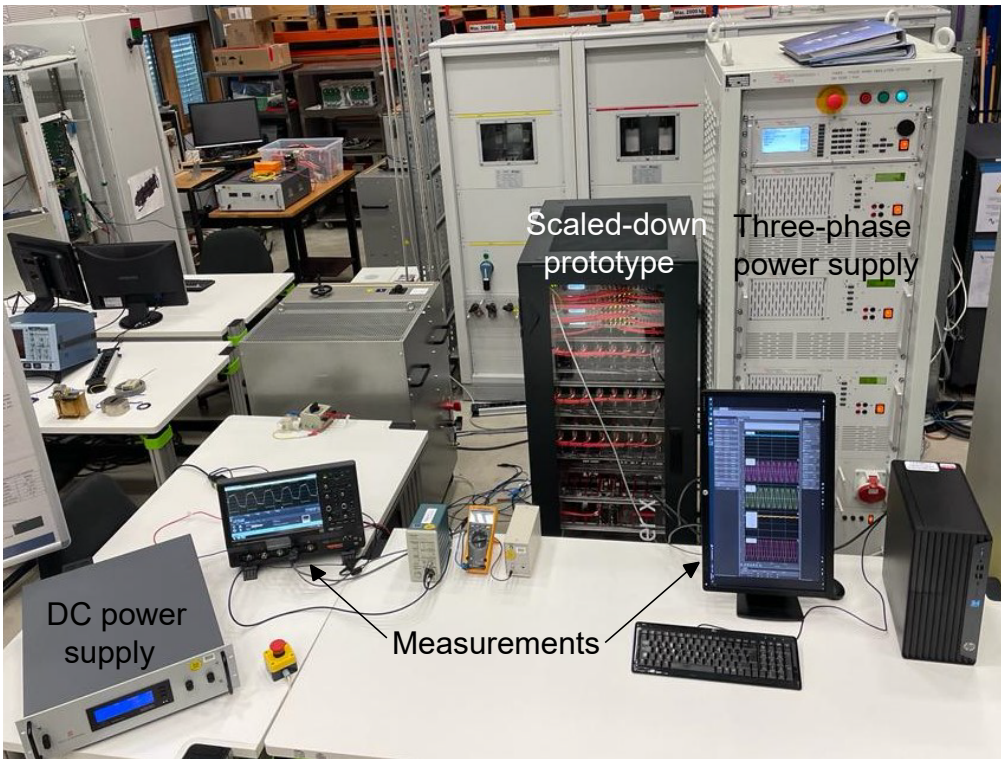

Fig. 3. Photograph of the experimental setup including a scaled-down MMC prototype.

TABLE I
RATINGS OF THE MMC-BASED SCALED-DOWN PROTOTYPE.

Description	Variable	Value	Unit
Output power	P_{out}	1	kW
Three-phase ac peak voltage	$\widehat{U}_y$	200	V
Single-phase ac peak voltage	$\widehat{U}_z$	200	V
DC voltage	u_{dc}	200	V
Summed capacitor voltage	V_y^x	400	V
Grid frequency	f_1	50	Hz
Single-phase frequency	f_2	1000	Hz
SM switching frequency	f_{sw}	5000	Hz
Arm inductance	L_y	2.36	mH
Arm capacitance	C_y	1.25	mF
Ac/dc converter capacitance	C_{dc}	1	mF
Number of SMs per arm	N	4	-

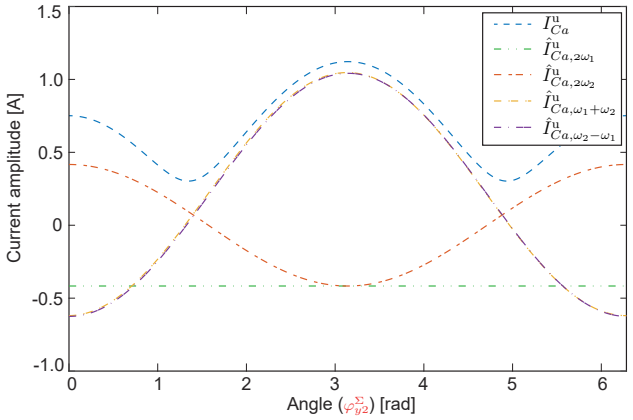

Fig. 4. SM capacitor RMS current and amplitudes in relation to φ_{y2}^{Σ}.

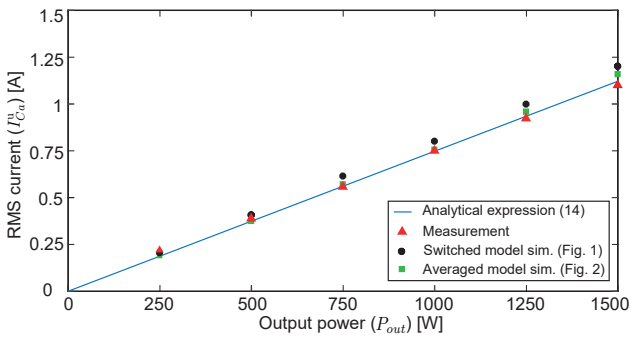

Fig. 5. SM capacitor RMS current in relation to the power.

and simulations using the switched and averaged circuit models as shown in Fig. 5. The expression in (14) is confirmed by varying the converter output power (P_{out}) for a fixed $\varphi_{y2}^{\Sigma} = 0.1$ rad. The error between the analytical expression, simulations and measurements in Fig. 5 can be attributed to the closed-loop control to obtain (9) and losses that were not considered in the model.

To verify (15) and (16), the relation between ripple voltage and sub-module capacitance is presented in Fig. 6. Simulation results from the switched and averaged models are plotted together with the measurement in a scaled-down prototype. The differences between the switched and averaged models are due to the additional ripple caused by the SM switching frequency. The PWM and sorting algorithm to select the insertion indices of SMs in the MMC arms contribute with high frequency components

that are not present in the averaged model. The voltage ripple from simulations and measurement in Fig. 6 is calculated as presented in Fig. 11, which also shows the high frequency components. Furthermore, the models do not include the dead-time between switches that also contributes to the voltage ripple, which could explain the deviation of the measured ripple.

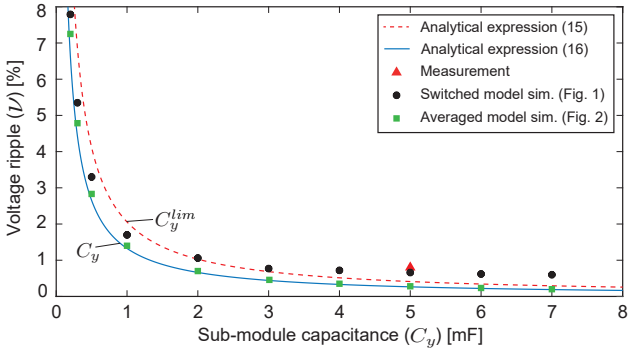

Fig. 6. Capacitor voltage ripple in relation to the sub-module capacitance.

The SM capacitance is fixed in the experimental setup, which limits the ripple measurement to one point in Fig. 6. The switched model exhibits greater precision than the averaged model in comparison to the measurement. Therefore, the capacitor current and voltage analysis should consider PWM and dead-time for better capacitance evaluation in ac/ac MMCs.

As presented in Fig. 7, the insertion indices in (9) are comprised of common-mode and differential-mode components. The closed-loop control modifies (9) with the measurements of summed capacitor voltage ripple instead of its average value. Since the summed capacitor voltage in the experimental setup is higher than in (10), the MMC arms are under-modulated.

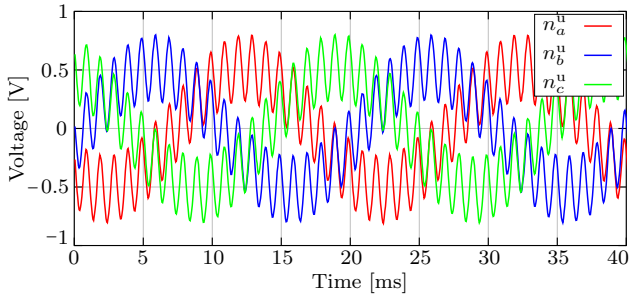

Fig. 7. Upper arm insertion index.

Since the MMC arms are interfacing both the three-phase AC grid and single-phase MFT, the steady-state upper arm currents measurements shown in Fig. 8 include frequencies ω_1 and ω_2.

Fig. 9 compares the simulated averaged model and measured SM capacitor currents to verify the amplitudes in (14). In the experiments the capacitor currents (i_{Cy}^x) cannot be readily measured, so they have been derived from the measured arm currents (Fig. 8), through multiplication

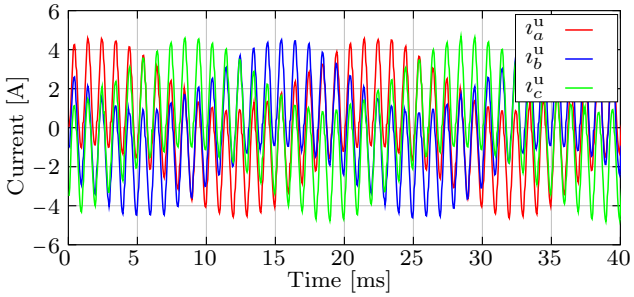

Fig. 8. Upper arm current measurements.

with the arm insertion indices (Fig. 7) that are obtained with a closed-loop control.

Fig. 10 shows the Fast Fourier Transform (FFT) of simulation and measurement from Fig. 9. The FFT confirms the current amplitudes presented in Fig 4. However, the closed-loop control that generates the arm insertion indices introduces undesired harmonics in the SM capacitor current [17]. Furthermore, the operation point of φ_{y2}^{Σ} in Fig. 4 could explain the mismatch between current amplitudes of simulation and experiment.

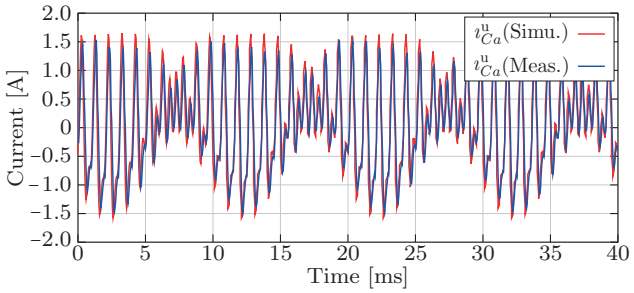

Fig. 9. SM capacitor current simulation and measurement (multiplication of n_y^x and i_y^x).

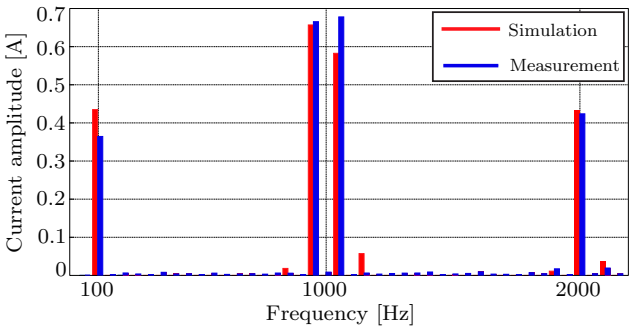

Fig. 10. Simulated and measured spectra of the SM capacitor current.

The SM capacitor voltage measurement is plotted in Fig. 11 together with the simulation result. The switched model was used for an accurate comparison with the measurement. The high frequency components in the voltage ripple are associated to the PWM and sorting algorithm that modifies (9).

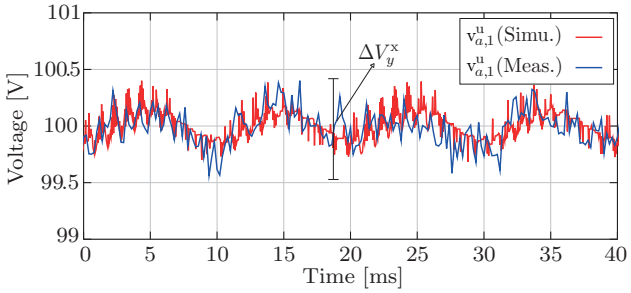

Fig. 11. SM capacitor voltage simulation and measurement.

V. Conclusion

This paper evaluates the capacitor RMS current and voltage ripple in full-bridge SMs of a direct three-phase to single-phase ac/ac MMC. Based on the capacitor voltage in the SMs, the required capacitance for a specific voltage ripple was determined. As a result, the analysis can be utilized to dimension SM capacitance in ac/ac MMCs, which is a driving factor of the size and cost in many applications.

Experiments show the arm currents of the MMC with frequency components from the three-phase and single-phase terminals. Furthermore, simulation and measurement of the capacitor current and voltage ripple in one sub-module attest the analysis.

Acknowledgments

This publication is part of the project NEON (with project number 17628 of the research programme Crossover which is (partly) financed by the Dutch Research Council (NWO)).

References

[1] Y. P. Marca, M. G. L. Roes, J. L. Duarte, and K. G. E. Wijnands, "Isolated MMC-based ac/ac stage for ultrafast chargers," in *30th International Symposium on Industrial Electronics*. IEEE, 2021, pp. 01–08.

[2] Y. P. Marca, M. G. L. Roes, J. L. Duarte, and K. G. E. Wijnands, "Square wave operation to reduce pulsating power in isolated MMC-based ultrafast chargers," in *24th European Conference on Power Electronics and Applications*. IEEE, 2022, pp. 1–7.

[3] K. Pouresmaeil, J. Duarte, K. Wijnands, M. Roes, and N. Baars, "Single-phase bidirectional ZVZCS AC-DC converter for MV-connected ultra-fast chargers," in *PCIM Europe 2022; International Exhibition and Conference for Power Electronics, Intelligent Motion, Renewable Energy and Energy Management*. VDE, 2022, pp. 124–130.

[4] T. Nakanishi and J.-i. Itoh, "Capacitor volume evaluation based on ripple current in modular multilevel converter," in *2015 9th International Conference on Power Electronics and ECCE Asia (ICPE-ECCE Asia)*. IEEE, 2015, pp. 815–822.

[5] M. A. Perez, S. Ceballos, G. Konstantinou, J. Pou, and R. P. Aguilera, "Modular multilevel converters: Recent achievements and challenges," *IEEE Open Journal of the Industrial Electronics Society*, vol. 2, pp. 224–239, 2021.

[6] K. Sharifabadi, L. Harnefors, H.-P. Nee, S. Norrga, and R. Teodorescu, *Design, control, and application of modular multilevel converters for HVDC transmission systems*. John Wiley & Sons, 2016.

[7] H. Bärnklau, A. Gensior, and S. Bernet, "Submodule capacitor dimensioning for modular multilevel converters," *IEEE Transactions on Industry Applications*, vol. 50, no. 3, pp. 1915–1923, 2013.

[8] R. Marquardt, A. Lesnicar, J. Hildinger *et al.*, "Modulares stromrichterkonzept für netzkupplungsanwendung bei hohen spannungen," *ETG*, vol. 114, pp. 155—161, 2002.

[9] R. Marquardt, "A new modular voltage source inverter topology," in *6th European Conference on Power Electronics and Applications*, 2003, pp. 1–10.

[10] K. Ilves, S. Norrga, L. Harnefors, and H.-P. Nee, "On energy storage requirements in modular multilevel converters," *IEEE transactions on power electronics*, vol. 29, no. 1, pp. 77–88, 2013.

[11] Y. Tang, L. Ran, O. Alatise, and P. Mawby, "Capacitor selection for modular multilevel converter," *IEEE Transactions on Industry Applications*, vol. 52, no. 4, pp. 3279–3293, 2016.

[12] M. Vasiladiotis, N. Cherix, and A. Rufer, "Accurate capacitor voltage ripple estimation and current control considerations for grid-connected modular multilevel converters," *IEEE Transactions on Power Electronics*, vol. 29, no. 9, pp. 4568–4579, 2013.

[13] J. Kolb, F. Kammerer, and M. Braun, "Dimensioning and design of a modular multilevel converter for drive applications," in *2012 15th International Power Electronics and Motion Control Conference (EPE/PEMC)*. IEEE, 2012, pp. LS1a–1.1–1–LS1a–1.1–8.

[14] M. M. Merlin and T. C. Green, "Cell capacitor sizing in multilevel converters: cases of the modular multilevel converter and alternate arm converter," *IET Power Electronics*, vol. 8, no. 3, pp. 350–360, 2015.

[15] M. Zygmanowski, B. Grzesik, and R. Nalepa, "Capacitance and inductance selection of the modular multilevel converter," in *2013 15th European conference on power electronics and applications (EPE)*. IEEE, 2013, pp. 1–10.

[16] Z. Liu, K.-J. Li, J. Wang, Z. Javid, M. Wang, and K. Sun, "Research on capacitance selection for modular multi-level converter," *IEEE Transactions on Power Electronics*, vol. 34, no. 9, pp. 8417–8434, 2018.

[17] L. Bessegato, K. Ilves, L. Harnefors, S. Norrga, and S. Östlund, "Control and admittance modeling of an ac/ac modular multilevel converter for railway supplies," *IEEE transactions on power electronics*, vol. 35, no. 3, pp. 2411–2423, 2019.

[18] S. P. Engel and R. W. De Doncker, "Control of the modular multilevel converter for minimized cell capacitance," in *Proceedings of the 2011 14th European Conference on Power Electronics and Applications*, 2011, pp. 1–10.

[19] J. Hu, M. Xiang, L. Lin, M. Lu, J. Zhu, and Z. He, "Improved design and control of FBSM MMC with boosted AC voltage and reduced DC capacitance," *IEEE Transactions on Industrial Electronics*, vol. 65, no. 3, pp. 1919–1930, 2017.

[20] P. Dong, J. Lyu, and X. Cai, "Optimized design and control for hybrid MMC with reduced capacitance requirements," *IEEE Access*, vol. 6, pp. 51 069–51 083, 2018.

[21] Q. Li, B. Li, J. He, E. Prieto-Araujo, D. W. Spier, H. Lyu, and O. Gomis-Bellmunt, "A novel design of circulating current control target to minimize SM capacitance in MMC," *International Journal of Electrical Power & Energy Systems*, vol. 143, p. 108432, 2022.

[22] T. Younis, P. Mattavelli, P. Magnone, I. Toigo, and M. Corradin, "Enhanced level-shifted modulation for a three-phase five-level modified modular multilevel converter (MMC)," *IEEE journal of emerging and selected topics in power electronics*, vol. 10, no. 1, pp. 704–716, 2021.